

Discretionary Lane-Change Decision and Control via Parameterized Soft Actor-Critic for Hybrid Action Space

Yuan Lin¹, Xiao Liu^{2,*}, Zishun Zheng³, and Liyao Wang⁴

¹ Shien-Ming Wu School of Intelligent Engineering, South China University of Technology, Guangzhou 510641, China; yuanlin@scut.edu.cn

² Shien-Ming Wu School of Intelligent Engineering, South China University of Technology, Guangzhou 510641, China; 202121060431@mail.scut.edu.cn

³ Shien-Ming Wu School of Intelligent Engineering, South China University of Technology, Guangzhou 510641, China; 202320160023@mail.scut.edu.cn

⁴ Shien-Ming Wu School of Intelligent Engineering, South China University of Technology, Guangzhou 510641, China; 202320160010@mail.scut.edu.cn

* Correspondence: 2943532919@qq.com

Abstract: This study focuses on a crucial task in the field of autonomous driving, autonomous lane change. Autonomous lane change plays a pivotal role in improving traffic flow, alleviating driver burden, and reducing the risk of traffic accidents. However, due to the complexity and uncertainty of lane-change scenarios, the functionality of autonomous lane change still faces challenges. In this research, we conduct autonomous lane-change simulations using both Deep Reinforcement Learning (DRL) and Model Predictive Control (MPC). Specifically, we propose the Parameterized Soft Actor-Critic (PASAC) algorithm to train a DRL-based lane-change strategy to output both discrete lane-change decision and continuous longitudinal vehicle acceleration. We also use MPC for lane selection based on predictive car-following costs for different lanes. For the first time, we compare the performance of DRL and MPC in the context of lane-change decision. Simulation results indicate that, under the same reward/cost functions and traffic flow, both MPC and PASAC achieve a collision rate of 0%. PASAC demonstrates comparable performance to MPC in terms of episodic rewards/costs and average vehicle speeds.

Keywords: Reinforcement learning; Hybrid action space; Lane change; Model Predictive Control

1. Introduction

The development of autonomous driving has indeed brought revolutionary changes to transportation[1]. Autonomous driving technology not only alleviates the burden on drivers and improves traffic flow but, more importantly, significantly reduces traffic accidents caused by human errors in driving. According to the World Health Organization, nearly 1.3 million people die in road traffic accidents globally each year, with 94% attributed to driver errors. Especially in lane-change scenarios, the actions of surrounding vehicles are often challenging to predict, making automated lane-change a critical task for autonomous vehicles.

Research indicates that nearly 10% of highway accidents are caused by lane-change maneuvers[2]. Therefore, a safe, smooth, and efficient automated lane-change mechanism is crucial for autonomous vehicles. To achieve this goal, the vehicle's architecture must possess efficient and robust execution capabilities, able to handle uncertainties in the operating environment, make wise decisions, and execute appropriate actions to cope with potential adversarial or cooperative behaviors of surrounding vehicles.

Currently, automated lane-change in autonomous driving is considered as Level 2 automation, indicating a relatively high degree of automation[3]. Advanced driver-assistance systems such as Lane Keeping Assist (LKA), Lane Centering Control (LCC), and Adaptive Cruise Control (ACC)[4] are relatively well-established, but the lane-change function still requires further development and breakthroughs. Although there has been some progress in researching automated lane-change decision-making, this functionality has not yet been widely implemented in vehicles.

Citation: Yuan Lin, Xiao Liu*, Zishun Zheng, and Liyao Wang. Discretionary Lane-Change Decision and Control via Parameterized Soft Actor-Critic for Hybrid Action Space. *Preprints* 2023, 1, 0. <https://doi.org/>

Copyright: © 2024 by the author. Submitted to *Preprints* for possible open access publication under the terms and conditions of the Creative Commons Attribution (CC BY) license (<https://creativecommons.org/licenses/by/4.0/>).

In the field of MPC stands out for its method of optimizing a sequence of future control actions to address real-time control problems. For instance, Ji proposed a collision-free trajectory planning method based on artificial potential fields and multi-constraint MPC[6]. Raffo presented an MPC-based trajectory tracking method, with two cascaded MPC controllers handling vehicle kinematics and dynamics models, effectively reducing computational complexity[7]. Xu introduced an MPC controller for a lane-keeping system, utilizing a five-point interpolation method to generate a reference trajectory[8]. Similarly, Sameul conducted simulations comparing MPC and PID controllers for trajectory tracking in autonomous vehicles, finding that MPC exhibited better robustness in various scenarios, including vehicle load, longitudinal velocity, and steering changes[9]. Hang proposed a human-like decision-making framework, combining potential field methods and MPC for collision-free path planning, providing predicted motion states for the human-like decision-making module. Additionally, he introduced a module that integrates decision-making and motion planning, considering the social behavior of surrounding traffic participants[10-11].

On the other hand, reinforcement learning (RL) has consistently been a research hotspot in the field of decision-making. For instance, the AlphaGo Go-playing robot, which defeated the human Go champion, is a result of training in discrete-action reinforcement learning[12]. Currently recognized discrete-action reinforcement learning algorithms include Deep Q-Network (DQN)[11], Double DQN (DDQN)[13], Rainbow[14], among others. Continuous-action reinforcement learning algorithms include Deep Deterministic Policy Gradient (DDPG)[15], Twin-Delayed DDPG (TD3)[16], Soft Actor Critic (SAC)[17], and so on. Few papers have proposed different methods to obtain hybrid action spaces[18]. One highly cited method is Parameterized DDPG (PA-DDPG), introduced in 2016 by scholars from the University of Texas, which utilizes continuous-action reinforcement learning to address hybrid action spaces[19]. Another well-cited method is Parameterized Deep Q-Network (PDQN), proposed in 2018 by researchers from Tencent AI Lab, which combines actor-critic learning and Q-learning, utilizing Q-learning instead of critic learning in DDPG for discrete action selection[20]. In 2019, scholars from the University of Twente proposed an improved approach called Multi-pass P-DQN (MPDQN)[21], which distributes continuous action inputs to the Q-network based on the correspondence between discrete and corresponding continuous actions, resulting in more reasonable Q-value outputs. In 2022, scholars from Tianjin University introduced the HyAR-TD3 algorithm[22], which employs representation learning to map continuous action spaces and hybrid action spaces.

Currently, most literature uses discrete reinforcement learning to achieve optimal control for non-mandatory automated lane-change in autonomous vehicles[23-27]. Typically, these papers adopt a hierarchical control approach, where the upper-level control outputs lane-change decisions using discrete reinforcement learning (discrete control variables), and the lower-level control uses a car-following model to output vehicle acceleration (continuous control variables). However, only a few studies have applied hybrid-action reinforcement learning to automated lane-change decision-making and control. In 2021, scholars from the University of Washington proposed the Hybrid Deep Q-Learning and Policy Gradient (HDQPG) to achieve automated lane-change in vehicles[28].

In this paper, we present an enhancement to the SAC continuous-action reinforcement learning algorithm, introducing the PASAC algorithm tailored for hybrid-action spaces. We train the model using traffic simulation software on the SUMO platform for various traffic scenarios. To validate the algorithm's superior performance in terms of stability and optimality, we compare the results of PASAC with MPC, considering metrics such as collision rate, average speed, value function, and jerk. However, it is crucial to note some known differences between the two approaches. Firstly, MPC requires online optimization and demands relatively powerful computing resources for real-time applications, raising cost concerns in practical deployment [29], which requires hardware-in-the-loop simulation to verify real-time readiness. On the other hand, the offline-trained DRL solution, based on neural networks, has short computation times and is suitable for real-time applications.

Secondly, MPC relies on a model-based approach, while DRL control solutions, based on black-box neural networks, lack theoretical guarantees [30].

In our MPC model, the ego vehicle needs to assess whether executing a lane-change maneuver is beneficial. If deemed beneficial, it adjusts its position and speed to prepare for the lane change; otherwise, it chooses to follow the preceding vehicle. In RL, the intelligent agent interacts with the environment, selects actions based on the current state, and continually updates its policy based on environmental feedback in the form of rewards. The intelligent agent in reinforcement learning can learn adaptive driving strategies for lane-change problems, enabling vehicles to make more intelligent lane-change decisions.

The primary contribution of this work is the introduction of the PASAC algorithm based on the SAC algorithm and the first quantitative and comprehensive comparison of the hybrid-action space reinforcement learning algorithm with MPC. We experimentally verify the superiority of PASAC in lane-change decision and control and conduct a detailed analysis of its performance. To the best of our knowledge, such a comparison does not exist in the literature. This not only provides new insights into the application of hybrid-action space reinforcement learning in practical control problems but also offers empirical support for the comparison of reinforcement learning with traditional control methods.

Regarding the paper structure, the second section provides a detailed introduction of the PASAC algorithm. The application of PASAC and MPC in lane-change scenarios is discussed in the third and fourth sections, respectively. The fifth section compares the DRL and MPC methods. Finally, conclusions are drawn in the sixth section.

2. Parameterized Soft Actor-Critic

In this section, we provide an overview of the hybrid action space structure in the SAC algorithm.

2.1. Reinforcement learning

Reinforcement learning is a learning method employed for decision-making and control. In reinforcement learning, an agent takes actions based on the current time step's environmental state, and subsequently, the environment transitions to a new state in the next time step as a result of that action. The agent also receives rewards based on the actions taken, and both the actions and rewards have a certain degree of probabilistic nature. The objective of reinforcement learning algorithms is to learn effective policies by minimizing the expected discounted cumulative reward for each episode. Specifically, the discounted cumulative reward for a state-action pair is referred to as the Q-value, denoted as $Q(\mathbf{s}_t, \mathbf{a}_t) = \mathbb{E}[\sum_{\tau=t}^T \gamma^{\tau-t} r(\mathbf{s}_\tau, \mathbf{a}_\tau)]$. Here, $r(\mathbf{s}_\tau, \mathbf{a}_\tau)$ represents the reward for the state s and action a at time step τ , and $\gamma \in [0,1]$ is the discount factor. The resolution of reinforcement learning problems adheres to the Bellman Optimality Principle. This principle asserts that if the optimal Q-value for the next step is known, then the action for the current time step must also be optimal. In other words, for an optimal policy, $Q(\mathbf{s}_t, \mathbf{a}_t)^* = r(\mathbf{s}_t, \mathbf{a}_t) + \gamma Q^*(\mathbf{s}_{t+1}, \mathbf{a}_{t+1})$, with $*$ denoting the optimality. This principle forms the foundation for devising effective policies in reinforcement learning.

2.2. Soft Actor-Critic

The Actor-Critic architecture is a core component of the RL algorithm, as proposed by Sutton and Barto (1999)[31]. It is used to solve action selection and value function learning. In this context, we consider a parameterized state value function V , a soft Q function, and a policy network. The parameters of these networks are denoted as ψ , $\hat{\psi}$, θ and ϕ respectively. The SAC algorithm considers the maximum entropy objective in reinforcement learning's maximum expectation, and the modified expectation is

$$J(\pi) = \sum_{t=0}^T \mathbb{E}_{(\mathbf{s}_t, \mathbf{a}_t) \sim \rho_\pi} \gamma^t [r(\mathbf{s}_t, \mathbf{a}_t) + \alpha H(\pi(\cdot | \mathbf{s}_t))], \quad (1)$$

In the formula, "." represents all possible actions. ρ_π denotes the new policy. The higher the entropy H , the stronger the system's uncertainty. In other words, a policy with higher entropy provides more significant action unpredictability. To regulate the impact of entropy on the policy, the SAC algorithm introduces a hyperparameter α , which plays a pivotal role in determining the relative significance of the entropy term on rewards.

$$\pi^* = \arg \max_{\pi} \mathbb{E}_{\tau \sim \pi} \left[\sum_{t=0}^{\infty} \gamma^t (R(\mathbf{s}_t, \mathbf{a}_t, \mathbf{s}_{t+1})) + \alpha H(\pi(\cdot | \mathbf{s}_t)) \right], \quad (2)$$

In this context, the introduction of an independent soft value function approximator not only enhances training stability but also facilitates concurrent training with other neural networks. The primary objective in training the soft value function is to minimize the square of residuals. In essence, through the optimization of the soft value function, the goal is to diminish the disparity between model predictions and actual observations, thereby enhancing the overall efficacy of the training process.

$$J_V(\psi) = \mathbb{E}_{\mathbf{s}_t \sim D} \left[\frac{1}{2} (V_\psi(\mathbf{s}_t) - E_{\mathbf{a}_t \sim \pi_\psi} [Q_\theta(\mathbf{s}_t, \mathbf{a}_t) - \log \pi_\phi(\mathbf{a}_t | \mathbf{s}_t)])^2 \right], \quad (3)$$

The gradient can be estimated using an unbiased estimator

$$\hat{\nabla}_\psi J_V(\psi) = \nabla_\psi V_\psi(\mathbf{s}_t) (V_\psi(\mathbf{s}_t) - Q_\theta(\mathbf{s}_t, \mathbf{a}_t) + \log \pi_\phi(\mathbf{a}_t | \mathbf{s}_t)), \quad (4)$$

The parameters of the soft Q-value function are determined by minimizing the residual of the Bellman equation.

$$J_Q(\theta) = \mathbb{E}_{(\mathbf{s}_t, \mathbf{a}_t) \sim D} \left[\frac{1}{2} (Q_\theta(\mathbf{s}_t, \mathbf{a}_t) - \hat{Q}(\mathbf{s}_t, \mathbf{a}_t))^2 \right], \quad (5)$$

with

$$\hat{Q}(\mathbf{s}_t, \mathbf{a}_t) = r(\mathbf{s}_t, \mathbf{a}_t) + \gamma \mathbb{E}_{\mathbf{s}_{t+1} \sim p} [V_{\hat{\psi}}(s_{t+1})], \quad (6)$$

After optimizing with stochastic gradient

$$\hat{\nabla}_\theta J_Q(\theta) = \nabla_\theta Q_\theta(\mathbf{s}_t, \mathbf{a}_t) (Q_\theta(\mathbf{s}_t, \mathbf{a}_t) - r(\mathbf{s}_t, \mathbf{a}_t) - \gamma V_{\hat{\psi}}(s_{t+1})), \quad (7)$$

The method of translating strategies using neural networks is as follows

$$\mathbf{a}_t = f_\phi(\epsilon_t; \mathbf{s}_t), \quad (8)$$

ϵ_t represents an input noise vector sampled from a fixed distribution, such as a spherical Gaussian distribution. The objective function denoted as

$$J_\pi(\phi) = \mathbb{E}_{\mathbf{s}_t \sim D, \epsilon_t \sim N} [\log \pi_\phi(f_\phi(\epsilon_t; \mathbf{s}_t) | \mathbf{s}_t) - Q_\theta(\mathbf{s}_t, f_\phi(\epsilon_t; \mathbf{s}_t))], \quad (9)$$

Where π_ϕ is defined by the function f_ϕ , the gradient of Equation 9 is as follows:

$$\hat{\nabla}_\phi J_\pi(\phi) = \nabla_\phi \log \pi_\phi(\mathbf{a}_t | \mathbf{s}_t) + (\nabla_{\mathbf{a}_t} \log \pi_\phi(\mathbf{a}_t | \mathbf{s}_t) - \nabla_{\mathbf{a}_t} Q(\mathbf{a}_t, \mathbf{s}_t)) \nabla_\phi f_\phi(\epsilon; \mathbf{s}_t). \quad (10)$$

2.3. Parameterized Soft Actor-Critic

In this context, we have defined a Markov Decision Process with a parameterized action space. The action space consists of a set of discrete actions, denoted as $A_d = a_1, a_2, \dots, a_n$. Each discrete action $a \in A_d$ is associated with a corresponding set of continuous parameters, represented as $a_1^{p_1}, a_2^{p_2}, \dots, a_n^{p_n}$. In our environment, the Actor network outputs m continuous parameters to form continuous actions and selects $n - m$ continuous parameters as weights for the discrete actions ($m < n$). The discrete action is determined by choosing the action with the maximum weight among the $n - m$ continuous parameters,

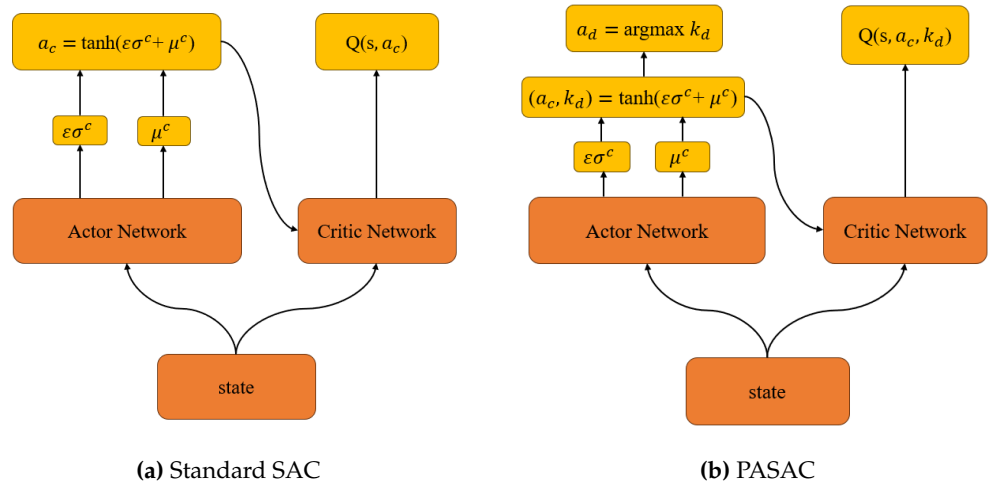


Figure 1. (a) The framework on the left is the standard SAC architecture designed for continuous operation. The actor outputs mean and standard deviation vectors μ and σ , which are utilized for injecting standard normal noise ϵ and applying the tanh nonlinearity (to keep the actions within a bounded range). The critic estimates their corresponding Q value based on the state and the actor's action a_c . (b) On the right, we propose the parameterized SAC structure, including the mean μ and the variance σ for the continuous components. It outputs continuous actions a_c and k_d . The larger-weighted k_d among continuous actions is selected as the discrete action. The critic network still takes the state s , continuous actions a_c and k_d as inputs.

expressed as $a_d = \max(am + 1, am + 2, \dots, a_n)$. The role of the Actor network is to simultaneously decide which discrete action to execute and how to parameterize that action. Here, we have adopted an approach similar to Delalleau 2019[32], but unlike the former, our discrete actions are deterministic rather than stochastic.

The PASAC algorithm is similar to the algorithm proposed by Peter Stone in 2016[19], as illustrated below: The Actor neural network can directly output continuous actions, and for discrete actions, it outputs the action with the maximum weight, where the weights are normalized within the range $[0, 1]$. The training process of PASAC algorithm is shown in Algorithm 1.

In order to gain a comprehensive understanding of the decision-making process of the PASAC algorithm, we will provide a detailed explanation of its neural network framework. Refer to Figure 1 for an illustration. In the structure diagram, the agent has two branches for handling actions—one for processing continuous actions and another for processing discrete actions. The outputs of these two branches are integrated into the final action decision, enabling the agent to learn and execute tasks in a mixed-action space.

3. PASAC for Lane Change

In this section, we utilize the open-source simulator SUMO [33] in conjunction with the Python library "flow," developed by Kheterpal (2018)[34]. This integrated framework is employed to construct the RL environment, governing the behavior of autonomous vehicles. We present a model for autonomous lane change based on reinforcement learning. By explicitly modeling states, actions, and rewards, the objective is to realize intelligent lane-change decisions for vehicles navigating through intricate traffic scenarios.

3.1. Scenario settings

In the conducted experiments detailed in this paper, we utilized a straight roadway with a length of 1000 meters and two lanes. A typical lane change scenario in SUMO as shown in Fig 2, the red car represents the ego vehicle, while the green cars represent the surrounding vehicles.

Algorithm 1 PASAC Algorithm Training Process.

Input: $\theta, \psi, \hat{\psi}, \phi$
 $\hat{\psi} \leftarrow \psi, D \leftarrow \emptyset$
For each iteration do
 For each environment step do
 $(\mathbf{a}_c, \mathbf{k}_d) \sim \pi_\phi(\mathbf{a}_t | \mathbf{s}_t)$
 $\mathbf{a}_d \sim \text{argmax } \mathbf{k}_d$
 $\mathbf{s}_{t+1} \sim p(\mathbf{s}_{t+1} | \mathbf{s}_t, \mathbf{a}_t)$
 $D \leftarrow D \cup \{(\mathbf{s}_t, \mathbf{a}_t, \mathbf{r}(\mathbf{s}_t, \mathbf{a}_t), \mathbf{s}_{t+1})\}$
 End for
 For each gradient step do
 $\theta_i \leftarrow \theta_i - \lambda_Q \hat{\nabla}_{\theta_i} J_Q(\theta_i)$ for $i \in \{1, 2\}$
 $\phi \leftarrow \phi - \lambda_\pi \hat{\nabla}_\phi J_\pi(\phi)$
 $\psi \leftarrow \psi - \lambda_V \hat{\nabla}_\psi J_V(\psi)$
 $\hat{\psi}_i \leftarrow \tau \psi_i + (1 - \tau) \hat{\psi}_i$ for $i \in \{1, 2\}$
 End for
End for
Output θ, ψ, ϕ

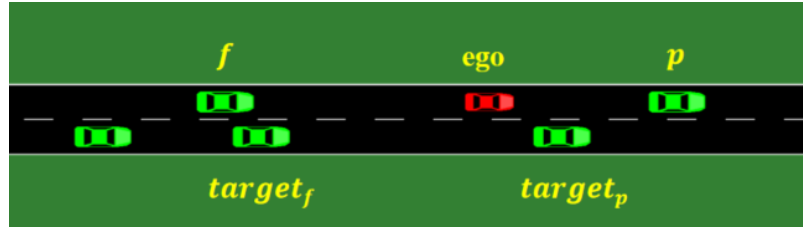


Figure 2. Lane change scenario in SUMO

3.2. State

At time t , the distance between the ego vehicle and the preceding vehicle d_t^p , the distance between the ego vehicle and the following vehicle d_t^f , the distance from the ego vehicle to the preceding vehicle in the target lane $d_t^{\text{target}_p}$, the distance from the ego vehicle to the following vehicle in the target lane $d_t^{\text{target}_f}$, ego vehicle's speed v_{ego} , ego vehicle's acceleration a_t^{ego} , The speeds of the preceding car and following car v_t^p, v_t^f , as well as the speeds of the preceding and trailing cars in the target lane $v_t^{\text{target}_p}, v_t^{\text{target}_f}$.

$$s = (d_t^p, d_t^f, d_t^{\text{target}_p}, d_t^{\text{target}_f}, v_t^{\text{target}_p}, v_t^{\text{target}_f}, v_t^{\text{ego}}, a_t^{\text{ego}}, v_t^p, v_t^f) \in S \quad (11)$$

3.3. Action

In general, making intelligent lane-change decisions in complex traffic environments involves assessing whether the lane change is beneficial. In this context, we define the action space as

$$a = \{a_t^{\text{ego}}, 0, 1\} \in A, \quad (12)$$

In Equation (12), the symbol '0' signifies a choice to postpone the lane change, indicating the intent to maintain the current position within the ego lane. Conversely, the symbol '1' represents an immediate decision to execute the lane change, manifesting the intention to promptly transition to the target lane. These symbols denote discrete actions. ' a_t^{ego} ', on the other hand, is a continuous action representing the rate of change of velocity.

3.4. Reward

The reward function is crafted with the objective of motivating positive behaviors and discouraging undesirable actions within the decision-making process of autonomous vehicles. In this paper, distinct rewards are allocated for tasks such as distance control, successful lane changes, adherence to speed limits, and collision avoidance. Drawing upon this concept, we have formulated the following reward function.

$$R_{total} = R_{act} + R_{act1} + R_{act2} + R_{collision} \quad (13)$$

where R_{total} is the total reward for the simulation scene. Where $R_{collision}$ is the penalty for vehicle collisions.

$$R_{act} = -\omega_0 |y_{t-1} - y_t| \quad (14)$$

In equation (14), R_{act} is the penalty for frequent lane changes by vehicles, w_0 is the corresponding weight, y_t and y_{t-1} represent the current and previous time step's longitudinal positions of the vehicle. Note that when the distance to the preceding vehicle satisfies the ACC spacing, this reward penalty will not be computed, thus aligning with the MPC cost function.

Through a comprehensive analysis of the disparity between the actual speed and the desired speed of the ego vehicle, coupled with meticulous management of the spacing between the ego vehicle and its preceding and following counterparts, we have skillfully crafted a longitudinal acceleration control strategy. The primary aim of this strategy is to mitigate the likelihood of collisions between vehicles, strategically initiating lane-change maneuvers during instances of reduced speed in the ego vehicle, thereby further optimizing the overall travel time. In consideration of passenger comfort, we have implemented a penalty mechanism for changes in longitudinal acceleration, seeking to strike a harmonious balance between driving efficiency and the overall passenger experience. The specific reward function is delineated as follows:

$$R_{act1} = -\omega_1 |d_t^p - d_{safe}| - \omega_2 |d_t^f - d_{safe}| \quad (15)$$

$$R_{act2} = -\omega_3 |v_{ego} - v_{safe}| - \omega_4 |jerk| \quad (16)$$

In equations (15) and (16), w_1 , w_2 , w_3 , and w_4 denote the corresponding weights. Here, d_{safe} represents the desired safe distance, v_{safe} is the desired safe speed, and $jerk$ signifies the rate of change of acceleration for the ego vehicle.

In order to comprehensively present the key parameters involved in our analysis, we introduce a parameter table (Table 1) at this point.

Table 1. Simulation lane change scene parameters.

Parameters	Value	Weights	Value
a_{min}	-4.5m/s ²	w_0	3.13
a_{max}	2.6m/s ²	w_1	0.5
v_{safe}	13.89m/s	w_2	0.4
d_{safe}	25m	w_3	0.72
$R_{collision}$	-200	w_4	0.5

4. Model Predictive Control Model

In MPC, the control inputs are determined by solving an optimization problem at each time step, taking into account the current state of the system and predicting its evolution over the horizon. This optimization process aims to minimize a predefined cost function. Here, we compare the costs for different lanes and initial a lane change for the lane with the lowest cost. The lane change is instantaneous wherein no lateral control is considered.

It's worth noting that we use YALMIP to handle optimization solutions. By leveraging the open-source solver YALMIP, we formulate and solve the MPC optimization problem.

YALMIP can be installed in MATLAB, providing programmers with various shooting and optimization methods to address nonlinear optimization problems. In this section, the principles of decision control for the self-driving vehicle under MPC are introduced. It includes the state-space equations, cost function, constraints, future state estimation, and variable-spacing strategy.

4.1. State-space equations

The state-space equation serves as a pivotal mathematical tool for describing the behavior of dynamic systems, playing a crucial role in control theory, system modeling, and engineering applications. The state-space equation for the MPC we have implemented as follows.

$$x = [d_t^p, d_t^f, \Delta v_t^p, \Delta v_t^f, j_t^{ego}, a_t^{ego}, v_{ego}] \quad (17)$$

$$u = a \quad (18)$$

$$x(k+1) = \mathbf{A}x(k) + \mathbf{B}u(k) \quad (19)$$

with

$$\mathbf{A} = \begin{bmatrix} 1 & 0 & -T_s & T_s & 0 & 0 & 0 \\ 0 & 1 & T_s & 0 & -T_s & 0 & 0 \\ 0 & 0 & 1 & 0 & 0 & T_s & 0 \\ 0 & 0 & 0 & 1 & 0 & 0 & 0 \\ 0 & 0 & 0 & 0 & 1 & 0 & 0 \\ 0 & 0 & 0 & 0 & 0 & 0 & 0 \\ 0 & 0 & 0 & 0 & 0 & -1/T_s & 0 \end{bmatrix}, \mathbf{B} = \begin{bmatrix} 0 \\ 0 \\ 0 \\ 0 \\ 0 \\ 1 \\ 1/T_s \end{bmatrix}, \quad (20)$$

In Formula, x is utilized as the input, where d_t^p and d_t^f denote the distances to the preceding and following vehicles, respectively. The variables Δv_t^p and Δv_t^f represent the velocity differences with the preceding and following vehicles, while v_{ego} , j_t^{ego} , and a_t^{ego} denote the velocity, acceleration, and jerk of the vehicle, respectively. u represents the control variable, where T_s is the time interval, with T_s set to 0.1 seconds.

4.2. Cost function

$$J = \omega_1 |d_t^p - d_{safe}| + \omega_2 |d_t^f - d_{safe}| + \omega_3 |v_{ego} - v_{safe}| + \omega_4 |jerk| \quad (21)$$

Formula(21) is consistent with the PASAC reward function.

4.3. Variable-spacing strategy

The following distance strategy can be mainly categorized into constant following distance strategy and variable following distance strategy. The constant following distance strategy fails to balance multiple control objectives, is unable to adapt to complex and changing driving scenarios, and results in excessive following distances at low speeds. These drawbacks contribute to a low acceptance of ACC systems employing a constant following distance strategy. To address the limitations of the constant following distance strategy, the variable following distance strategy adjusts the following distance based on driving scenarios. One typical approach is the safety distance strategy based on the following time gap and can be expressed as follows:

$$d_{safe} = d_0 + v_t^{ego} t_p \quad (22)$$

In the formula, d_{safe} represents the desired following distance, d_0 represents the safe distance between the ego vehicle and the lead vehicle when the ego vehicle is stationary, and t_p represents the time gap during following. These parameters are constants, while v_t^{ego} represents the velocity of the ego vehicle, with its speed changes being minimal. Therefore, we approximate d_{safe} as a fixed value.

4.4. TLACC(Two-Lane Adaptive Cruise Control)

TLACC is the Decision and Control Algorithm of MPC.

Algorithm 2 TLACC Algorithm Process.

Input: $d_t^p, d_t^f, \Delta v_t^p, \Delta v_t^f, a_t^{ego}, j_t^{ego}, l_t^c, v_{ego}$
Onput: u_d, l_{sw}

While TLACC engaged **do**
 $(J_c, u_d^c) \leftarrow \text{MPC}(d_t^p, d_t^f, \Delta v_t^p, \Delta v_t^f, a_t^{ego}, j_t^{ego}, l_t^c, v_{ego})$
 If $J_c \leq J_{th}$ **Then**
 Return $l_{sw} \leftarrow 0, u_d \leftarrow u_d^c$
 else
 $(J, u_{target}) \leftarrow \text{MPC}(d_{target}^p, d_{target}^f, \Delta v_{target}^p, \Delta v_{target}^f, a_t^{ego}, j_t^{ego}, l_{target}, v_{ego})$
 If $(1 + k_p)J \leq J_c$ **Then**
 Return $l_{sw} \leftarrow 1, u_d \leftarrow u_{target}$
 else
 Return $l_{sw} \leftarrow 0, u_d \leftarrow u_d^c$
 End
End
End

Where J_c and J denote the future driving costs on the current lane and the target lane, respectively. l_{sw} is the lane change signal, where 0 indicates staying in the current lane, and 1 indicates a change to the target lane. J_{th} is the threshold value for the future driving cost on the current lane that must be satisfied for a lane change, with J_{th} set to 0.8. u_d^c is the desired control input, and u_d and u_{target} are the expected control inputs for driving on the current lane and the target lane, respectively. k_p is the penalty term for the future driving cost during a lane change, with k_p set to 0.1.

5. Comparison results of DRL and MPC

Under the consistent conditions of relevant hyperparameters, cost functions, input states, and traffic flow, this section presents the test results of DRL and Model Predictive Control MPC controllers.

5.1. DRL training

For the training of the reinforcement learning model, we chose a simulation timestep of 300,000, with each timestep set to 0.1 seconds. The training was conducted on a computer equipped with an 8-core (16-thread) AMD processor and an NVIDIA GeForce RTX 3050 Ti GPU, and the training process took approximately 3 hours. It is noteworthy that, before the start of each episode, there is a 50-meter buffer for the initialization of main-road traffic.

In our study, to achieve effective training of the reinforcement learning model, we meticulously selected and configured a set of crucial hyperparameters. The choice of these hyperparameters directly impacts the model's performance and the stability of the training process. In Table 2, we provide a detailed list of the hyperparameters utilized during training along with their corresponding values.

Table 2. Parameterized SAC Hyperparameters.

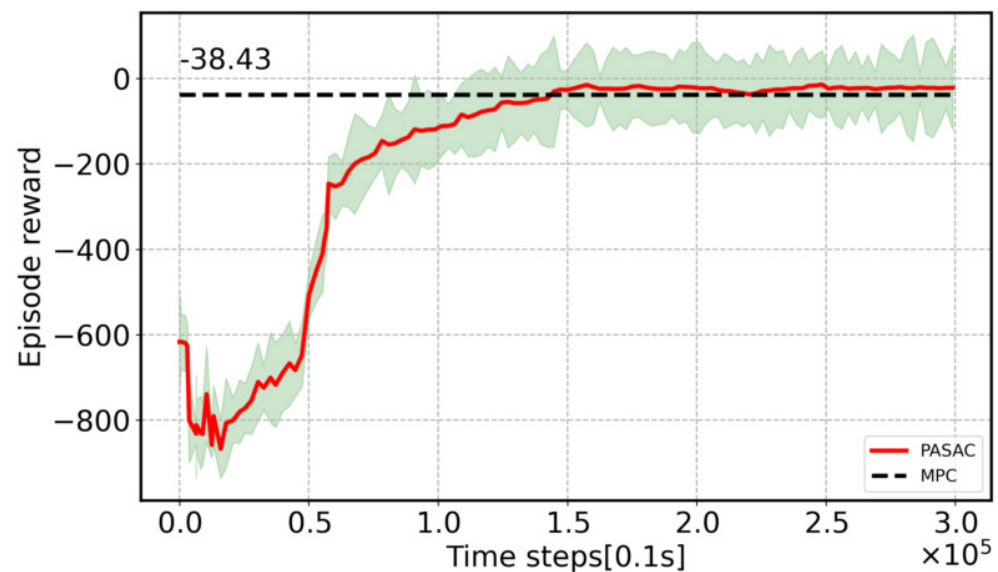
Hyperparameters	Value	Hyperparameters	Value
Discount factor	0.99	Tau	0.005
Alpha	0.05	Learn starts	500
Mini-batch size	128	Buffer size	10000
Actor learning rate	0.0001	Train freq	1
Critic learning rate	0.001	Gradient steps	1

5.2. DRL testing

The trained policy underwent additional testing with an extended 350,000 simulation time steps, representing 500 episodes. In order to better assess the performance of the model, we selected a typical initial condition where the leading vehicle's initial velocity was set to 12.89 m/s, and the ego vehicle's initial velocity was set to 13.89 m/s, with a traffic flow density of 0.11.

5.3. Comparison and Analysis

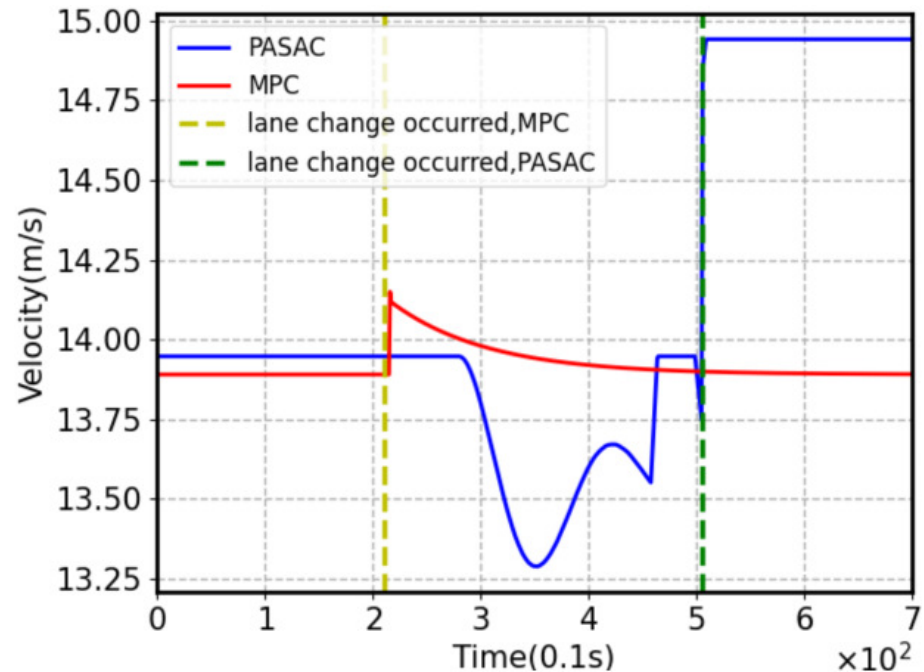
In the preceding chapters, MPC has been applied to lane-change scenarios in autonomous driving, effectively leveraging its strengths in dynamic system modeling and solving optimization problems. In contrast, RL employs a learning approach based on reward functions, allowing the intelligent agent to improve its behavior through trial and error, adapting to complex driving tasks. In the following sections, we will compare the performance of MPC and RL in executing lane-change tasks for autonomous vehicles.

**Figure 3.** The cost between MPC and PASAC

In Figure 3, the solid line represents the training curve of PASAC, and it can be observed that it approaches convergence around 150,000 steps. The dashed line represents the sum of values trained over 700 steps in MPC. (One episode of PASAC training takes approximately 700 steps) The performance comparison results between PASAC and MPC are shown in Table 3. Note that in collision-free scenarios, the average speed and cost function of vehicles in PASAC are superior to MPC. This implies that PASAC achieves better speed and time benefits.

Table 3. Comparison of Results from 500 Episodes of Testing

	Collision	Average speed(m/s)	Cost
PASAC	0%	14.34	-27.58
MPC	0%	13.95	-38.43

**Figure 4.** Lane change in the simulation.

In Figure 4, the red solid line represents the self-driving vehicle controlled by the MPC method, while the deep blue solid line represents the vehicle controlled by the reinforcement learning algorithm PASAC. In PASAC, the vehicle decelerates suddenly and then accelerates, while in MPC, it accelerates first and then decelerates. The green and yellow dashed lines respectively represent lane changes by the self-driving vehicle under PASAC and MPC.

It can be observed that lane changes in PASAC and MPC occur at different times (MPC occurs around 22s, while PASAC occurs around 51s). This is because, for PASAC and MPC, the vehicles are in different states before the sudden lane change occurs. When they reach the location where the lane change and sudden speed change occur, different driving scenarios are generated. The self-driving vehicle under PASAC changes lanes immediately after a sudden deceleration, then accelerates to maintain a higher speed, obtaining more travel time benefits. On the other hand, the self-driving vehicle under MPC changes lanes after a sudden acceleration, maintaining a stable speed and adopting a relatively conservative approach.

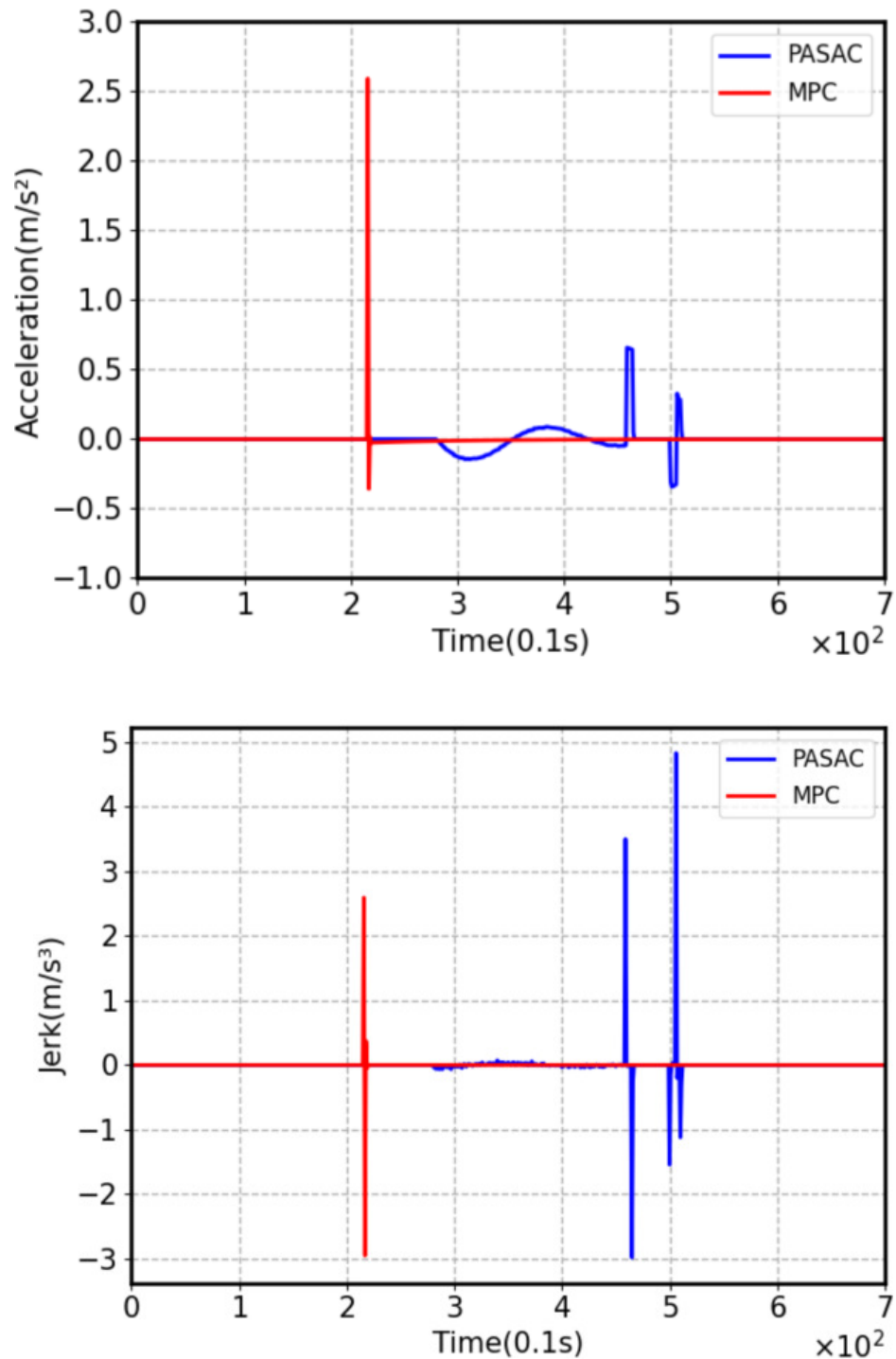


Figure 5. Acceleration and jerk during the simulation

In the simulation results depicted in Figure 5, the acceleration and jerk of both MPC and PASAC demonstrate smooth motion characteristics, avoiding abrupt accelerations and vibrations, significantly enhancing the comfort of the driver. Figures 6 and 7 depict the longitudinal position and distance to the leading vehicle in the simulations of PASAC and MPC for the ego vehicle.

6. Conclusions

In this study, we proposed a novel hybrid-action reinforcement learning algorithm, PASAC, and conducted MPC in the decision and control problems of autonomous vehicles during the lane-change process. DRL training and MPC optimization were based on the

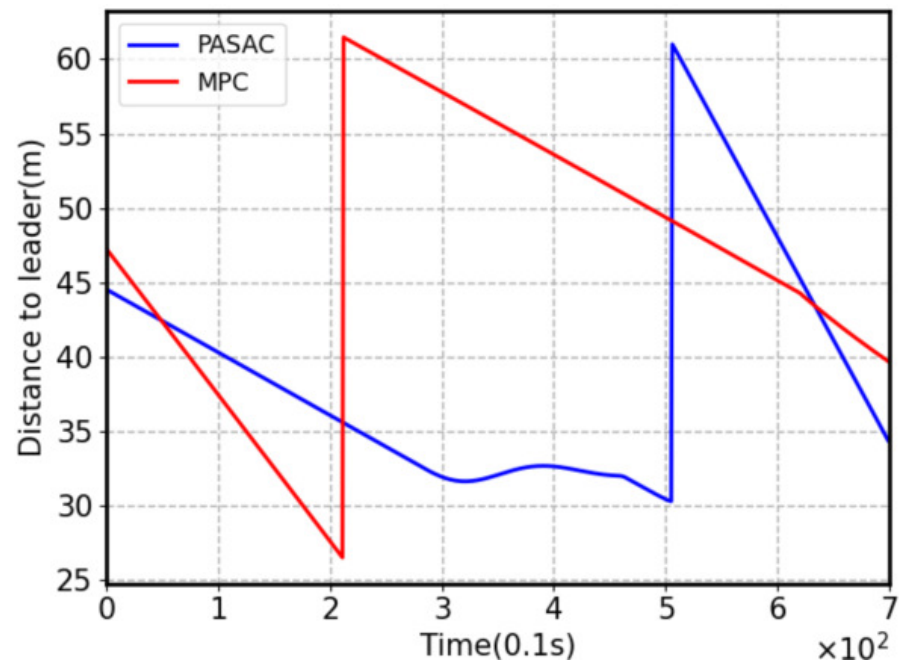


Figure 6. The figure illustrates the distance from the ego vehicle to the leading vehicle, with a set safety following distance of 25 meters. To optimize safety benefits, both MPC and PASAC choose to initiate lane changes before reaching the 25-meter distance to the leading vehicle. Note that there is a sudden change in the distance between the ego vehicle and the leading vehicle, indicating a successful lane change and a subsequent alteration in the state of the leading vehicle.

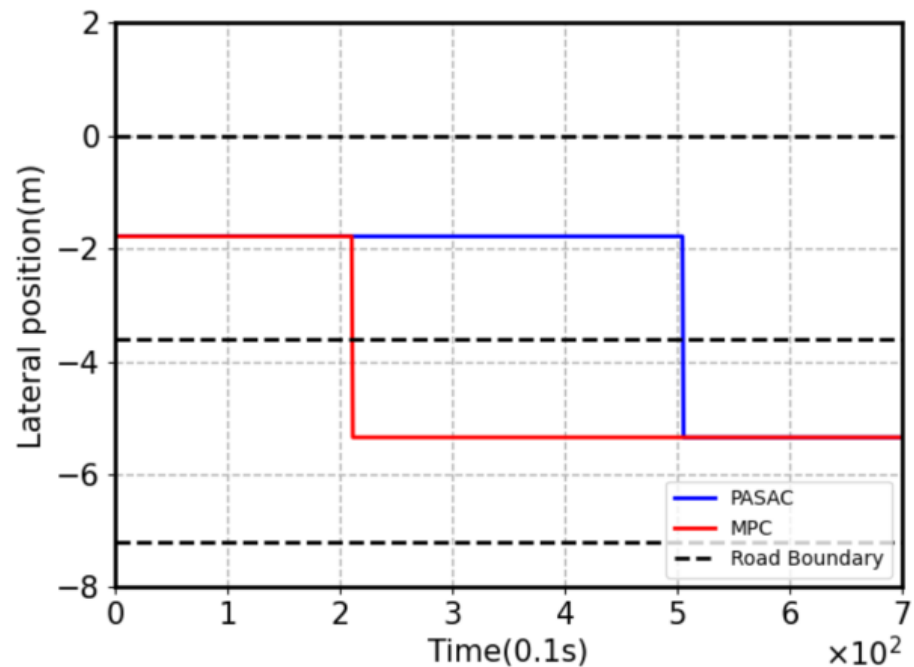


Figure 7. The figure illustrates the longitudinal position of the autonomous vehicle on the road, with dashed lines representing the road boundaries and solid lines distinctly outlining the precise location of the vehicle along the centerline of the road. Here, we assume that the vehicle is traveling along the prescribed lane. Through the visual contrast between the dashed and solid lines, we can clearly observe whether the vehicle remains within the drivable area of the road. This helps evaluate the performance of the autonomous driving system in longitudinal control, ensuring that the vehicle consistently stays within a safe and compliant zone during its journey.

same action space equations and value functions. They shared the same control update frequency and were capable of handling hybrid-action space problems. We maintained identical testing conditions for PASAC and MPC, including traffic density and traffic scenarios. The results indicated that, in the absence of modeling errors, PASAC outperformed MPC in terms of the value function, particularly when an adequate prediction horizon was present. Furthermore, both PASAC and MPC exhibited a collision rate of 0%; however, PASAC required less time to complete the specified route. Nevertheless, the PASAC algorithm still encountered collisions in scenarios with higher traffic flow, and the potential reasons for this need further analysis. One of the challenges lies in the lack of theoretical analysis of the relationship between neural networks and optimal control, which could be a crucial area for future research.

Author Contributions: Conceptualization, Y.L.; methodology, X.L., Z.Z., and Y.L.; formal analysis, X.L., Y.L., and Z.Z.; investigation, X.L., Y.L.; data curation, X.L.; writing—original draft preparation, X.L.; writing—review and editing, L.Y., Y.L., X.L.; supervision, Y.L.; All authors have read and agreed to the published version of the manuscript.

Funding: Not applicable.

Institutional Review Board Statement: Not applicable.

Informed Consent Statement: Not applicable.

Data Availability Statement: The data can be obtained upon reasonable request from the corresponding author.

Conflicts of Interest: The authors declare that they have no known competing financial interest or personal relationships that could have appeared to influence the work reported in this paper.

References

1. Urmson, C., Anhalt, J., Bagnell, D., Baker, C., Bittner, R., Clark, M.N., Dolan, J., Duggins, D., Galatali, T., Geyer, C. and Gittleman, M. Autonomous driving in urban environments: Boss and the urban challenge. *Journal of Field Robotics*. 2008. **25**(8). 425-466.
2. Hetrick, S. Examination of driver lane change behavior and the potential effectiveness of warning onset rules for lane change or “side” crash avoidance systems. Dissertation, Virginia Polytechnic Institute & State University. 1997.
3. Nilsson, J., Brännström, M., Coelingh, E. and Fredriksson, J. Lane change maneuvers for automated vehicles. *IEEE Transactions on Intelligent Transportation Systems*. 2016. **18**(5). 1087-1096.
4. Li, S., Li, K., Rajamani, R., et al. Model predictive multi-objective vehicular adaptive cruise control. *IEEE Transactions on Control Systems Technology*. 2010. **19**(3). 556-566.
5. Yu, S., Hirche, M., Huang, Y., et al. Model predictive control for autonomous ground vehicles: a review. *Autonomous Intelligent Systems*. 2021. **1**(1). 4.
6. Ji, J., Khajepour, A., Melek, W. W., et al. Path Planning and Tracking for Vehicle Collision Avoidance Based on Model Predictive Control With Multiconstraints. *IEEE Transactions on Vehicular Technology*. 2017. **66**(2). 952-964.
7. Raffo, G. V., Gomes, G. K., Normey-Rico, J. E., et al. A Predictive Controller for Autonomous Vehicle Path Tracking. *IEEE Transactions on Intelligent Transportation Systems*. 2009. **10**(1). 92-102.
8. Xu, Y., Chen, B. Y., Shan, X., et al. Model predictive control for lane keeping system in autonomous vehicle. In *2017 7th International Conference on Power Electronics Systems and Applications - Smart Mobility, Power Transfer & Security (PESA)*. Hong Kong: IEEE, 2017. 1-5.
9. Samuel, M., Mohamad, M., Hussein, M., et al. Lane keeping maneuvers using proportional integral derivative (PID) and model predictive control (MPC). *Journal of Robotics and Control (JRC)*. 2021. **2**(2). 78-82.
10. Hang, P., Lv, C., Xing, Y., et al. Human-Like Decision Making for Autonomous Driving: A Noncooperative Game Theoretic Approach. *IEEE Transactions on Intelligent Transportation Systems*. 2021. **22**(4). 2076-2087.
11. Hang, P., Lv, C., Huang, C., et al. An Integrated Framework of Decision Making and Motion Planning for Autonomous Vehicles Considering Social Behaviors. *IEEE Transactions on Vehicular Technology*. 2020. **69**(12). 14458-14469.
12. Mnih, V., Kavukcuoglu, K., Silver, D., Rusu, A.A., Veness, J., Bellemare, M.G., Graves, A., Riedmiller, M., Fidjeland, A.K., Ostrovski, G. and Petersen, S. Human-level control through deep reinforcement learning. *Nature*. 2015. **518**(7540). 529-533.
13. Van Hasselt, H., Guez, A. and Silver, D. Deep reinforcement learning with double Q-learning. *Thirtieth AAAI Conference on Artificial Intelligence*. 2016. **30**(1). 2094-2100.
14. Hessel, M., Modayil, J., Van Hasselt, H., Schaul, T., Ostrovski, G., Dabney, W., Horgan, D., Piot, B., Azar, M. and Silver, D. Rainbow: Combining improvements in deep reinforcement learning. *Thirty-Second AAAI Conference on Artificial Intelligence*. 2018. **32**(1). 3215-3222.

15. Lillicrap, T.P., Hunt, J.J., Pritzel, A., Heess, N., Erez, T., Tassa, Y., Silver, D. and Wierstra, D. Continuous control with deep reinforcement learning. *International Conference on Learning Representations*. 2016.
16. Fujimoto, S., Hoof, H. and Meger, D. Addressing function approximation error in actor-critic methods. *International Conference on Machine Learning*. 2018. **80**. 1587-1596.
17. Haarnoja, T., Zhou, A., Abbeel, P. and Levine, S. Soft actor-critic: Off-policy maximum entropy deep reinforcement learning with a stochastic actor. *International Conference on Machine Learning*. 2018. **80**. 1861-1870.
18. Neunert, M., Abdolmaleki, A., Wulfmeier, M., Lampe, T., Springenberg, T., Hafner, R., Romano, F., Buchli, J., Heess, N. and Riedmiller, M. Continuous-discrete reinforcement learning for hybrid control in robotics. *Conference on Robot Learning*. 2019. 735-751.
19. Hausknecht, M. and Stone, P. Deep reinforcement learning in parameterized action space. *International Conference on Learning Representations*. 2016.
20. Xiong, J., Wang, Q., Yang, Z., Sun, P., Han, L., Zheng, Y., Fu, H., Zhang, T., Liu, J. and Liu, H. Parametrized deep Q-networks learning: Reinforcement learning with discrete-continuous hybrid action space. arXiv preprint arXiv:1810.06394. 2018.
21. Bester, C.J., James, S.D. and Konidaris, G.D. Multi-pass Q-networks for deep reinforcement learning with parameterised action spaces. arXiv preprint arXiv:1905.04388. 2019.
22. Li, B., Tang, H., Zheng, Y., Jianye, H.A.O., Li, P., Wang, Z., Meng, Z., & Wang, L.I. (2022). HyAR: Addressing Discrete-Continuous Action Reinforcement Learning via Hybrid Action Representation. *International Conference on Learning Representations*.
23. Mukadam, M., Cosgun, A., Nakhaei, A. and Fujimura, K. Tactical decision making for lane changing with deep reinforcement learning. 2017.
24. Wang, P., Chan, C.Y. and de La Fortelle, A. A reinforcement learning based approach for automated lane change maneuvers. *IEEE Intelligent Vehicles Symposium*. 2018. 1379-1384.
25. Alizadeh, A., Moghadam, M., Bicer, Y., Ure, N.K., Yavas, U. and Kurtulus, C. Automated lane change decision making using deep reinforcement learning in dynamic and uncertain highway environment. *IEEE Intelligent Transportation Systems Conference*. 2019. 1399-1404.
26. Saxena, D.M., Bae, S., Nakhaei, A., Fujimura, K. and Likhachev, M. Driving in dense traffic with model-free reinforcement learning. *IEEE International Conference on Robotics and Automation*. 2020. 5385-5392.
27. Wang G, Hu J, Li Z, et al. Harmonious lane changing via deep reinforcement learning. *IEEE Transactions on Intelligent Transportation Systems*. 2021. **23**(5). 4642-4650.
28. Guo, Q., Angah, O., Liu, Z., & Ban, X.J. (2021). Hybrid deep reinforcement learning based eco-driving for low-level connected and automated vehicles along signalized corridors. *Transportation Research Part C: Emerging Technologies*, 124, 102980.
29. M. Vajedi and N. L. Azad, "Ecological adaptive cruise controller for plug in hybrid electric vehicles using nonlinear model predictive control," *IEEE Trans. Intell. Transp. Syst.*, vol. 17, no. 1, pp. 113–122, Jan. 2016.
30. J. Lee, A. Balakrishnan, A. Gaurav, K. Czarnecki, and S. Sedwards, "Wisemove: A framework to investigate safe deep reinforcement learning for autonomous driving," in *Proc. Int. Conf. Quantitative Eval. Syst.*, 2019, pp. 350–354.
31. Sutton, R. S., & Barto, A. G. Reinforcement learning. *Journal of Cognitive Neuroscience* **1999**, 11(1), 126-134.
32. Delalleau, O., Peter, M., Alonso, E., et al. (2019). Discrete and continuous action representation for practical RL in video games. *arXiv preprint arXiv:1912.11077*.
33. D. Krajzewicz, J. Erdmann, M. Behrisch, et al. Recent development and applications of SUMO-Simulation of Urban MObility. *International Journal on Advances in Systems and Measurements*, 2012, **5**(3&4).
34. J. B. Nielsen, R. B. Thorolfsdottir, L. G. Fritsche, et al. Biobank-driven genomic discovery yields new insight into atrial fibrillation biology. *Nature Genetics*, 2018, **50**(9), 1234-1239.